

Complex environmental beta-plane turbulence: Laboratory Experiments with Altimetric Imaging Velocimetry

A. M. Matulka¹, Y. Zhang¹, and Y. D. Afanasyev¹

[1]{Memorial University of Newfoundland, St. John's, Canada}

Correspondence to: Y. D. Afanasyev (afanai@mun.ca)

Abstract

Results from the spectral analyses of the flows in two experiments where turbulent flows were generated in a rotating tank with topographic β -effect, are presented. The flows were forced either by heating water from below or supplying fresh water at the top of a saline layer. The flow was essentially barotropic in the first experiment and baroclinic in the second experiment. The gradient of the surface elevation was measured using optical altimetry (Altimetric Imaging Velocimetry). Multiple zonal jets of alternating direction were observed in both experiments. Turbulent cascades of energy exhibit certain universal properties in spite of the different nature of flows in the experiments.

1 Introduction

Two-dimensional β -plane turbulence is an important concept in complex environmental flows where planetary rotation and the effect of the variation of the Coriolis parameter with latitude (β -effect) are significant factors. Kraichnan (1967) formulated a Kolmogorov-type theory which predicted the slope $-5/3$ of the energy spectrum in the energy range and the slope -3 in the enstrophy range for two-dimensional turbulence. The β -effect modifies two-dimensional turbulence towards anisotropy. The energy spectra in wavenumber space become a figure-of-

1 eight with most of the energy concentrated at zonal wavenumber close to zero. In physical
2 space this effect manifests itself in the creation of zonal jets. Oceanographic observations of
3 this phenomenon have been extensively discussed in the literature (Maximenko et al., 2005,
4 2008; Centurioni et al., 2008; Ivanov et al. (2009)).

5 Experiments on the Coriolis rotating platform by Read et al. (2007) confirmed the
6 theoretical prediction of $-5/3$ slope in the energy range. The authors used convective forcing
7 in their experiments which generated motions of very small scale. Since the size of the
8 domain was large, the scale separation was large enough for the development of the inverse
9 cascade of energy. A recent study on two-dimensional turbulence (in the absence of β -effect)
10 by Afanasyev and Craig (2013) gave the experimental evidence of dual cascade with the
11 spectral slopes of $-5/3$ and -3 . Further experiments with barotropic turbulence on the β -plane
12 by Zhang and Afanasyev (2014) demonstrated the dual cascade in the presence of β -effect as
13 well as a “figure eight” energy spectrum in the wavenumber space.

14 Zonal jets have a long history of investigation starting from the pioneering experiments
15 by Whitehead (1975) and Colin de Verdiere (1979). The jets readily form when a spatially
16 localized forcing is applied in the β -plane fluid (e.g. Sommeria et al., 1988, 1989; Marcus and
17 Lee, 1998, Afanasyev et al., 2011, 2012; Slavin and Afanasyev, 2012). However, a distributed
18 forcing such as that provided by baroclinic instability, also creates jets. In the ocean, the
19 regions where baroclinic instability is dynamically important include the Antarctic
20 Circumpolar Current (ACC) as well as western boundary currents and their extensions.
21 Multiple jets as well as mesoscale eddies are created there by the baroclinic instability thus
22 forming a dynamically complex turbulent flow. A classic model for a baroclinically unstable
23 system is a rotating annulus where heating/cooling is provided at the outer wall/center of the
24 tank respectively. Different aspects of the dynamics of this system were studied in a number

1 of experiments (Hide and Mason, 1975; Mason, 1975; Bastin and Read, 1997, 1998;
2 Wordsworth et al., 2008; Smith et al., 2014). A somewhat different experimental approach to
3 modelling a baroclinically unstable two-layer flow with vertical shear was used in a recent
4 study by Matulka and Afanasyev (2015). It was shown that the meridional scale of the jets is
5 determined to large extent by the radius of deformation and, at the same time, is in good
6 agreement with the Rhines scale (Rhines, 1975). The jets are driven by (nonlinear) Reynolds
7 stresses due to baroclinic meanders. This is in agreement with a scenario described by Berloff
8 et al. (2009 a, 2009 b). The authors describe the formation of jets as a secondary instability of
9 the primary instability of the baroclinic flow in the form of mainly meridional motions (so-
10 called “noodles”).

11 In this study we perform spectral analyses of the flows described in Matulka and
12 Afanasyev (2015) and compare them with the results obtained for a somewhat different flow
13 generated by thermal forcing (Zhang and Afanasyev, 2014). The latter experiment although
14 forced baroclinically was more barotropic in its dynamics while the former experiment was
15 purely baroclinic. In Sec. II of this paper, we describe the laboratory setup for both
16 experiments. In Sec. III the results of the spectral analyses are reported. Concluding remarks
17 are given in Sec. IV.

18

19 **2 Experimental technique**

20 The laboratory experiments were carried out in a cylindrical tank of radius $R = 55$ cm filled
21 with water of depth $H_0 = 10 - 12$ cm. The tank was installed on a rotating table (Fig. 1 a) and
22 rotated in an anticlockwise direction at a constant angular rate $\Omega = 2.32$ rad/s. In this paper we
23 compare two experiments where the flows were forced in two different ways. The first
24 experiment was forced thermally with a heating wire at the bottom of the tank. The wire was

1 arranged in an approximately uniform pattern such that the distance between the segments of
 2 the wire was 4.5 cm. Figure 1 b shows the magnitude of velocity in the range between 0
 3 (black) and 0.5 cm/s (white) in the very beginning of the experiment. The flow is initially
 4 along the wires such that the wire pattern is visible. This wire arrangement (in contrast to,
 5 say, a spiral) was chosen in order to avoid a direct forcing in the zonal direction but yet to
 6 provide an approximately uniform mean heat flux across the bottom. The heater supplied the
 7 total power of 2300 W.

8 In the second experiment the flow was forced by delivering fresh water at the surface
 9 of a salt water layer of salinity $S = 30$ ppt. The fresh water source was distributed along the
 10 wall of the tank and created a coastal current flowing counterclockwise around the tank. The
 11 fresh water was pumped into the tank by a pump which delivered 20 liters of water in about 6
 12 min. Figure 1 c shows the camera view of the flow in the middle of the forcing period when
 13 the fresh water from the source has not yet spread over the entire surface of the tank but is
 14 concentrated mainly in the coastal current.

15 The free surface of the rotating fluid is a paraboloid when in solid-body rotation. The
 16 height of water surface varies quadratically with the distance r from the axis of rotation

$$17 \quad h(r) = H_0 + \frac{\Omega^2}{2g} \left(r^2 - \frac{R^2}{2} \right) \quad (1)$$

18 where g is the gravitational acceleration. This creates a topographic (polar) β -plane where the
 19 β -parameter at some distance $r = r_0$ from the pole is given by

$$20 \quad \beta = \frac{f_0}{h(r)} \frac{dh(r)}{dr} \Big|_{r=r_0} \quad (2)$$

21 where $f_0 = 2\Omega$ is the Coriolis parameter. The values of the β -parameter in our experiments
 22 were between 0.07 and 0.1 $\text{cm}^{-1}\text{s}^{-1}$.

1 We use the Altimetric Imaging Velocimetry (AIV) system to measure the gradient of
2 the surface elevation η (for more details see Afanasyev et al. 2009). AIV is based on optical
3 altimetry first described in Rhines et al. (2006). Laboratory altimetry is not unlike the satellite
4 altimetry which became an irreplaceable tool in oceanography. Apart from measuring $\nabla\eta$,
5 AIV can be used as a tool to visualize the entire surface of the rotating fluid just like satellite
6 altimetry provides a global coverage of the Earth's oceans. The AIV also provides an
7 alternative to a well-known Particle Imaging Velocimetry (PIV) technique. To obtain the
8 velocity field using PIV one has to find correlations between small areas (typically 12 – 48
9 pixels in both dimensions) of two successive images of the flow. If a camera has an imaging
10 array of size say 1000×1000 pixels, the resulting array of velocity vectors has dimensions less
11 than 100×100 . Thus, the PIV technique effectively reduces the spatial resolution by a factor
12 of 100 or more. AIV, on the other hand, allows one to obtain the velocity vector in every pixel
13 of the image, which makes its spatial resolution practically unlimited given that the cameras
14 with large imaging arrays are now easily available. The limitation of the AIV is that it can
15 only be used in a relatively fast rotating fluid with free surface. It is, however, perfectly suited
16 for oceanographic fluid dynamics experiments on the β -plane as those described in this paper.
17 Paraboloidal surface of the rotating fluid is used like the mirror of a Newtonian telescope. If
18 the surface is disturbed by the pressure perturbations due to the flow, the slope of the surface
19 changes slightly. These perturbations of the slope are detected by the AIV and measured
20 using simple geometry and a color coding.

21 AIV measures an “exact” (within experimental accuracy) surface elevation gradient,
22 $\nabla\eta$, which translates into the pressure gradient, $\nabla p = \rho g \nabla\eta$, at the surface. Note that the
23 main uncertainty is due to the color noise of the camera sensor. To reduce the noise we pass
24 data through a median filter with a window size of 5×5 pixels (physical size of approximately

1 0.2×0.2 cm). The overall uncertainty of $\nabla\eta$ can be estimated to be approximately 5%. The
 2 velocity field is not measured directly by the AIV but rather obtained from the measured $\nabla\eta$
 3 using a (quasi-) geostrophic approximation.

4 The barotropic component of velocity can be calculated in geostrophic approximation
 5 as follows

$$6 \quad \mathbf{V} = \frac{g}{f_0}(\mathbf{n} \times \nabla \eta), \quad (3)$$

7 where \mathbf{n} is the vertical unit vector. A next order of approximation is provided by the quasi-
 8 geostrophy which gives

$$9 \quad \mathbf{V} = \frac{g}{f_0}(\mathbf{n} \times \nabla \eta) - \frac{g}{f_0^2} \frac{\partial}{\partial t} \nabla \eta - \frac{g^2}{f_0^3} J(\eta, \nabla \eta), \quad (4)$$

10 where J is the Jacobian operator. The second and the third terms in the RHS of Eq. (4) are
 11 corrections to the geostrophic velocity which take into account transient and nonlinear effects.
 12 Their relative importance is determined by the temporal Rossby number $Ro_T = 1/(f_0 T)$ and the
 13 Rossby number $Ro = U/(f_0 L)$ respectively. Here T is the time scale of the unsteady processes
 14 in the flow, while U and L are velocity and length scales of the flow. Thus, the velocity field
 15 is determined more accurately when the flow is closer to being quasigeostrophic. “Textbook”
 16 theory on the validity of the quasigeostrophic approximation applies here. Since the Rossby
 17 number did not exceed unity even in the core of the eddies in our experiments and the mean
 18 values of the Rossby number were of the order of 10^{-1} , the velocity was, on average, within
 19 10% of the “exact” velocity.

20 Relative vorticity, $\zeta = \mathbf{n} \cdot \text{curl} \mathbf{V}$, was calculated by differentiating the velocity field.
 21 Since numerical differentiation amplifies noise in the original data, we used the Sobel

1 gradient operators with 5×5 kernels (e.g. Pratt, 2007). The kernels are convolved with the
2 velocity data to calculate the derivatives in x- and y-directions.

3 According to the Taylor-Proudman theorem, the surface velocity given by Eq. (4) is a
4 good approximation for the velocity in the entire column of water except the Ekman layer at
5 the bottom. Note that in a stratified fluid, as in our two-layer experiment with saline forcing,
6 the velocity field obtained by altimetry is, in fact the barotropic component of the total
7 velocity in the entire layer of water. It is also the upper layer velocity. A baroclinic
8 component which allows one to obtain the total velocity in the lower layer can be measured
9 by a different technique (e.g. Afanasyev et al., 2009; Matulka and Afanasyev, 2015) but is not
10 discussed here.

11

12 **3 Results**

13 We performed two sets of experiments with different forcing, namely the thermal forcing by a
14 wire-heater at the bottom and the saline forcing by injection of fresh water at the wall. In what
15 follows we discuss them in parallel highlighting the similarities and differences between
16 them.

17 **3.1 General flow evolution**

18 Figure 2 a shows a typical snapshot of the surface of water in the experiment with the thermal
19 forcing when the flow is fully developed. The flow is visualized by the AIV technique such
20 that color shows the horizontal gradient of the surface elevation, $\nabla\eta$. The colour intensity
21 indicates the magnitude of $\nabla\eta$ while hue shows its direction. The motions are initially of
22 very small scale in this experiment (see also Fig. 1 b). Warm water heated by the wire rises to
23 the surface in thin sheets and forms long thin filaments. These filaments are unstable with

1 respect to baroclinic or frontal instability and break into small eddies. The size of the eddies is
 2 most likely determined by the baroclinic radius of deformation which can be defined as
 3 $R_d = (g' H_0 / 2)^{1/2} / f_0$, where g' is the reduced gravity in the warm water filaments and eddies.
 4 The reduced gravity is defined by the temperature difference between the water in filaments
 5 and background temperature of the water in the tank. However, since we did not measure the
 6 temperature field in this experiment, we cannot pinpoint the exact value of R_d . It is important
 7 to establish here the values of control parameters for the thermal convection in this
 8 experiment. Flows created by buoyancy sources in the rotating fluid (in the absence of the β -
 9 effect) were studied in laboratory experiments by Fernando et al. (1991) and Maxworthy and
 10 Narimusa (1994). The energy flux per unit area of the bottom of the tank is $Q = 2.5 \times 10^3$
 11 Wm^{-2} in our experiments. This translates into the buoyancy flux $B = \alpha g Q / C_p = 1.2 \times 10^{-6}$
 12 $\text{m}^2 \text{s}^{-3}$, where α is the thermal expansion coefficient and C_p is the volumetric heat capacity of
 13 water at constant pressure. A dimensionless parameter which controls the regime of the
 14 thermal convection is the Rayleigh number. The flux Rayleigh number is quite high in our
 15 experiments, $Ra_{flux} = B H_0^4 / \nu^2 \kappa = 1.8 \times 10^9$ (where κ is the thermal diffusivity of water) that
 16 indicates a regime of turbulent convection. Comparing to the recent experiments by Read et
 17 al. (2015) where similar heating was used but in an experiment of a larger scale, we note that
 18 our buoyancy flux was almost two orders of magnitude higher; the Rayleigh number was,
 19 however, an order of magnitude lower because of the smaller depth of water in our
 20 experiments.

21 Figure 3 a, b shows the fields obtained as a result of the velocity calculation from
 22 measured $\nabla \eta$ in the thermal experiment. Azimuthal velocity, V_{az} in a polar coordinate system
 23 with the origin at the center of the tank is shown in panel a, while panel b shows the relative
 24 vorticity, $\zeta = \mathbf{n} \cdot \text{curl} \mathbf{V}$. The relative vorticity field shows a fine structure of the flow with

1 multiple small scale cyclonic (red) and anticyclonic (blue) eddies. The relative vorticity is
2 normalized by the Coriolis parameter f_0 , thus the image in panel b can be interpreted as a map
3 of the Rossby number, $Ro = \zeta/f_0$. The values of Ro can reach unity in the strongest eddies
4 while the rms value is approximately 0.2. An original alignment of filaments with the heating
5 wires can still be seen in the central area of the tank while closer to the wall where the water
6 is deeper and the β -effect is stronger, the bands of positive and negative vorticity are aligned
7 in the zonal direction which indicates the presence of zonal jets. The jets can be seen more
8 clearly in the azimuthal velocity image in panel a. The circulation is mainly in the
9 counterclockwise (eastward) direction (V_{az} is positive, red color). Maximum values of V_{az} in
10 the jets are approximately 1 cm/s.

11 Figure 2 b and Figure 3 c, d (see also Fig. 1 c) show the experiment with the saline
12 forcing. The water in the tank is initially of salinity $S = 30$ ppt. When a source distributed
13 along the wall of the tank delivers fresh water, it creates a current along the wall. This current
14 is initially wedge-shaped in cross-section and is approximately in geostrophic balance such
15 that it „leans“ on the wall to its right. This coastal current can be seen clearly in Figures 1 c, 2
16 b and 3 c, the velocity of the current is initially in excess of 5 cm/s. The current is
17 baroclinically unstable (e.g. Griffiths and Linden, 1981) and creates meanders which
18 penetrate into the interior of the tank. During the forcing period of the experiment when the
19 source continuously supplies fresh water, the entire surface of the tank eventually becomes
20 covered with a layer of fresh water. Thus, a two-layer system is created. The forcing then
21 stops and the flow is allowed to develop freely. The depth of the upper layer is not uniform in
22 the radial direction after the period of forcing. The layer is much thicker at the wall of the tank
23 rather than at its center. Thus, the system contains a large amount of available potential
24 energy which is released gradually and maintains the flow for a very long time after the

1 forcing stops. The adjustment involves slow radial motion towards the center in the upper
2 layer and the motion in the opposite direction in the lower layer. The radial motion, in turn,
3 causes zonal circulation. Measurements of barotropic and baroclinic components of velocity
4 (for details see Matulka and Afanasyev, 2015) show that the upper layer rotates cyclonically
5 while the lower layer rotates anticyclonically. The shear between the layers makes the system
6 baroclinically unstable. Conditions for the development of the baroclinic instability are
7 maintained over a long period of adjustment. Note that measurements of mean energy and
8 enstrophy of the system (not shown here) during the long period of adjustment indicate that
9 the system is approximately steady in this experiment.

10 Baroclinic instability together with other instabilities including, perhaps, wave
11 breaking and barotropic and frontal instabilities, continuously generates meanders over the
12 entire area of the tank. The meanders move water parcels in the radial (meridional) direction.
13 According to conservation of potential vorticity the parcels acquire additional relative vorticity
14 and radiate Rossby waves. Motion of the meanders/parcels correlated via the global Rossby
15 wave field creates the Reynolds stresses which drive zonal jets in the interior of the tank.
16 Thus, although direct forcing was stopped, the system is forced by the baroclinic instability
17 similar to that in the ocean. Measurements of the Reynolds stresses in this experiment showed
18 that jets in the interior are dynamically different from the coastal jet which is affected by the
19 presence of the wall. The jets in the interior are true eddy-forced jets while the coastal current
20 is not. In what follows we perform spectral analyses of the flow in the inner area which
21 contains these “true“ jets and excludes the coastal current.

22 Visual comparison between the fields in the experiments with different forcing (Figure
23 3) shows that the scales of the turbulent eddies generated by the forcing are noticeably
24 different. The eddies in the thermal experiment are smaller which indicates smaller R_d .

1 Another difference is perhaps more significant in distinguishing between the forcing
2 mechanisms. The flow with saline forcing is characterised by thin filaments rather than
3 circular eddies. In fact, eddies appear only as a result of breaking of the filaments and do not
4 have very long lifetime. The filaments are created by the baroclinic instability; they protrude
5 in the radial (meridional) direction. We hypothesise that these filaments are the manifestation
6 of the so-called “noodles” which are the primary mode of the instability of the baroclinic flow
7 (Berloff et al., 2009 a, 2009 b).

8

9 **3.2 Energy spectra in wavenumber space**

10 Herein we describe the results of the spectral analysis of the flows. For a circular domain such
11 as our tank, it is perhaps more natural to use polar coordinates for the purpose of spectral
12 decomposition. Afanasyev and Wells (2005) used Fourier-Bessel transform to obtain two-
13 dimensional energy spectra of the polar β -plane turbulence in the space of azimuthal and
14 radial wavenumbers and then to obtain one-dimensional spectrum by sorting data in terms of
15 a polar analogue of the Cartesian isotropic wavenumber. However, it is easier to perform
16 digital Fourier decomposition in the Cartesian coordinates because Fast Fourier Transform
17 routines can be used. Moreover, usage of Cartesian coordinates and a conventional β -plane
18 (rather than quadratic polar β -plane) simplifies the further comparison with available theory.
19 For these reasons here we introduce a local Cartesian coordinates (x, y) centred at the
20 reference radius $r_0 = 25$ cm such that x-axis is directed to the east, $x = r_0\theta$ (where θ is the
21 polar angle) and y-axis is directed to the north, $y = r_0 - r$. For the spectral analyses we chose
22 a domain of half width 17 cm centred at the reference radius $r_0 = 25$ cm such that the polar
23 part of the tank, where β -plane approximation is inappropriate, and the wall area, where the
24 coastal jet dominates, were excluded.

1 The AIV technique gives velocity field on a regular rectangular grid covering the
 2 entire area of the tank. The velocity vector field was interpolated onto the local Cartesian
 3 coordinate system and then projected to eastward and northward directions to obtain zonal
 4 and meridional velocity components. Discrete Fourier transform of these velocity components
 5 then gives velocity $\mathbf{u}(k_x, k_y)$ in the wavenumber space (k_x, k_y) . The two-dimensional energy
 6 spectrum is given by

$$7 \quad E(k_x, k_y) = \frac{1}{2} |\mathbf{u}(k_x, k_y)|^2. \quad (4)$$

8 Figure 4 shows two-dimensional spectra in the experiments with thermal and saline
 9 forcing. The spectra are measured in the beginning of both experiments when the spectral
 10 signature of the forcing is still strong, and at a later stage, when the spectra reached certain
 11 “saturation” and the turbulent cascades are developed. The spectral properties of forcing or
 12 background turbulent flow can be inferred from the initial spectra. In the experiment with
 13 thermal forcing the eddies generated by thermal plumes are quite small; their scale can be
 14 estimated from the value of wavenumber $k \approx 2.5 \text{ cm}^{-1}$ (outer ring in Figure 4 a) to be
 15 approximately 2.5 cm. Here $k = (k_x^2 + k_y^2)^{1/2}$ is the isotropic wavenumber. These eddies are
 16 initially concentrated along the heating wires. The separation of the heating wires
 17 (approximately 4.5 cm) determines a wavenumber $k \approx 1.4 \text{ cm}^{-1}$ where energy concentration is
 18 observed as well (inner ring in Figure 4 a). In the experiment with saline forcing the initial
 19 spectrum is determined by the baroclinic instability which is sustained in the two-layer system
 20 even when the actual forcing (the injection of fresh water) is stopped. The energy is
 21 distributed in a wide range of wavenumbers but is mainly contained within a circle which
 22 corresponds to the reciprocal of the radius of deformation, $R_d^{-1} = 1.2 \text{ cm}^{-1}$. This is in
 23 agreement with the prediction of the Phillips model (Phillips 1951) of baroclinic instability.

1 The model predicts that all perturbations of wavenumber $k < R_d^{-1}$ are unstable with the most
2 unstable (before nonlinear saturation) wavenumber being $k = 0.64 R_d^{-1}$. Thus the initial spectra
3 for both experiments confirm our initial observation that the forcing scale is smaller in the
4 experiment with the thermal forcing. The spectra measured in much later times in both
5 experiments (Figure 4 b, d) show that energy cascades towards smaller wavenumbers (larger
6 scales). The distribution of energy in the wavenumber space also becomes more anisotropic;
7 the energy flows towards the k_y axis (zonal modes, $k_x = 0$).

8 The inverse energy cascade is a well-known phenomenon in two-dimensional
9 turbulence; energy is transferred from small scales (large k) to large scales (small k). In the
10 presence of β -effect, this scenario is modified. The pioneering work by Rhines (1975)
11 demonstrated that there is a certain scale, now known as the Rhines scale, which separates the
12 large-scale motions where β -effect dominates from a small-scale turbulence. A wavenumber
13 corresponding to the Rhines scale is given by

$$14 \quad k_R = \sqrt{\beta / U_{rms}} \quad , \quad (5)$$

15 where U_{rms} is root-mean-square velocity. On large scales Rossby wave elasticity is important
16 and the flow becomes strongly anisotropic as the (linear) dispersion relation for Rossby waves
17 suggests. The anisotropy is manifested by the appearance of zonal jets. The wavenumber k_R is
18 also widely used as an estimate for the meridional wavenumber of an arrangement of zonal
19 jets. It was shown to work well in different circumstances including flows on gas giants or
20 flows in the laboratory although different modifications of the Rhines scale were discussed as
21 well. The values of k_R for each experiment are indicated by crosses on y-axis in Figure 4 b, d.

1 To extend the Rhines' argument to two dimensions one can equate the frequency of
 2 turbulent eddies to that of Rossby waves to obtain (Vallis and Maltrud, 1993) a dividing line
 3 in the form

$$4 \quad k_8 = \sqrt{\frac{\beta \cos \theta}{U_{rms}}}, \quad (6)$$

5 where θ is the polar angle in the wavenumber space, $\theta = \arctan(k_y/k_x)$. The line given by (6)
 6 resembles a figure-of-eight or a dumbbell and is shown in Figure 4 b, d. Note that values of
 7 U_{rms} are not given by theory but have to be measured in the experiment. Here we used the
 8 rms values of the y-component of velocity instead of the total velocity in order to avoid the
 9 mean flow in the azimuthal direction which occurred to different extent in both of the
 10 experiments. Since Rhines' theory assumes isotropic small-scale turbulence, it seems that the
 11 y-component of velocity represents a better measure of turbulence in our case. Spectra in
 12 Figure 4 b, d show that the turbulent cascade of energy due to nonlinear interaction of modes
 13 does not continue in the isotropic manner within the area bounded by k_8 line. In fact, there is
 14 little energy inside this area. The energy follows instead a (linear) Rossby wave dispersion
 15 relation flowing along the k_8 line towards the k_y axis and concentrating there. It is eventually
 16 dissipated by friction which in our case is mainly the Ekman bottom friction which acts on all
 17 scales. The distribution of zonal energy indicates that the isotropic Rhines scale is indeed a
 18 reasonable measure of the jet wavenumber in both experiments.

19 To study general spectral characteristics of the turbulent cascade without regard to
 20 the anisotropy one can average energy over the polar angle θ in the wavenumber space. As a
 21 result, one obtains a one-dimensional energy spectrum which is defined as
 22 $E(k) = 2\pi k \langle E(\mathbf{k}) \rangle$, where $\mathbf{k} = (k_x, k_y)$ and the average is over $|\mathbf{k}| = k$. Figure 5 shows the
 23 one-dimensional spectra for our two experiments. Theory of two-dimensional turbulence

1 without β -effect predicts the existence of the dual cascade such that energy cascades to large
2 scales in the range $k < k_F$ with a Kolmogorov type spectral slope $-5/3$ and to small scales in
3 the range $k > k_F$ with a slope -3 . Here k_F is the forcing wavenumber where energy is injected
4 into the system. The former range is called the energy range while the latter is called the
5 enstrophy range. The forcing wavenumber can be estimated to be $k_F \approx 2.5 \text{ cm}^{-1}$ in the
6 experiment with thermal forcing and $k_F = 0.64 R_d^{-1} \approx 0.8 \text{ cm}^{-1}$ in the experiment with saline
7 forcing. These values mark the boundary between the energy and enstrophy ranges in both
8 experiments. Figure 5 shows that the spectral slope does change in the vicinity of the
9 estimated forcing wavenumbers that confirms that these estimates are meaningful. In both
10 experiments, $-5/3$ slope was observed in the energy range; in the first experiment (thermal
11 forcing) this range was longer than that in the second one (saline forcing). In the enstrophy
12 range the -3 slope was observed in the first experiment (thermal forcing) while the second
13 experiment (saline forcing) showed a much steeper slope. The presence of the -3 slope might
14 be another consequence of the mostly barotropic (and two-dimensional) character of the flow
15 in the first experiment. Indeed, the flow in this experiment is convectively unstable and
16 mixing is significant. As a result, the fluid is not significantly stratified and the flow must be
17 mainly barotropic. The steeper slope in the second experiment is, perhaps, due to the fact that
18 this two-layer, statically stable flow is significantly baroclinic. Note that steeper than -3 slope
19 was also measured in the experiments with shallow water, f-plane turbulence by Afanasyev
20 and Craig (2013) and in the numerical simulations by Yuan and Hamilton (1994).

21 The estimates of the Rhines wavenumber (accidentally) give similar values for both
22 experiments, $k_R \approx 0.45 \text{ cm}^{-1}$. This value indicates the place for zonal jets in the spectral
23 cascade. The maximum energy achieved by the cascade in the second experiment roughly
24 corresponds to the Rhines wavenumber which indicates that zonal motions should possess a

1 significant portion of the total energy. In the first experiment, the cascade does not quite reach
2 the Rhines wavenumber. Note that the Rhines wavenumber does not stop the cascade to even
3 lower wavenumbers; the cascade is just redirected towards zonal motions.

4

5 **4 Conclusions**

6 In our experiments we observed the formation of zonal jets in the experiments where flows
7 were forced using two different methods. Perhaps the main difference between the forcing
8 was that the heater at the bottom created convectively unstable vertical temperature
9 distribution which resulted in small scale convective plumes. Vertical mixing must be
10 significant in this system and the fluid remained mainly unstratified. The large scale flow in
11 this experiment is then approximately barotropic, although the nature of forcing is baroclinic.
12 In the second experiment, on the other hand, we created statically stable two-layer
13 stratification. The flow was baroclinic to a significant degree. Since this system was unstable
14 with respect to baroclinic instability, the instability as a source of small-scale turbulence.
15 Thus in both cases some small-scale turbulence was created but in the former experiment the
16 flow was mainly barotropic while in the latter it was mainly baroclinic.

17 In spite of this significant difference between the flows in our two experiments, we
18 observed a definite universality in their spectral dynamics. The energy cascaded from small
19 scales to larger scales and towards zonal motions. The two-dimensional spectra demonstrated
20 that this cascade is in reasonable agreement with the Rhines theory. One-dimensional spectra
21 of energy reliably demonstrated the existence of the energy interval with the $-5/3$ slope. Note
22 that although in our experiments one can infer the direction of the energy cascade from the
23 form of the spectrum assuming that the forcing wavenumber is known, direct evidence of the
24 cascade direction can only be provided by the analyses of the spectral energy flux. Such

1 evidence was provided for shallow water rotating turbulence (without β -effect) in the
2 laboratory investigation by Afanasyev and Craig (2013) The analysis of the energy flux for
3 the large-scale oceanic turbulence by Scott and Wang (2005) revealed the existence of the
4 inverse cascade in agreement with the two-dimensional turbulence theory. However, the
5 interplay between barotropic and baroclinic modes and the extent each mode contributes to
6 the cascade in the ocean still remains a subject of research. The analysis of the flux for the
7 experiments reported here is yet to be done and will be reported elsewhere.

8

9 **Acknowledgements**

10 The authors are grateful to Alexander Slavin for his help with one of the experiments. YDA is
11 supported by the Natural Sciences and Engineering Research Council of Canada.

12 Experimental data are available on request from Y. D. Afanasyev.

13

14 **References**

15 Afanasyev, Y. D., and Craig, J. D. C.: Rotating shallow water turbulence: experiments with
16 altimetry, *Phys. Fluids*, 25, 106603, doi:10.1063/1.4826477, 2013.

17 Afanasyev, Y. D., O’Leary, S., Rhines, P. B., and Lindahl, E. G.: On the origin of jets in the
18 ocean, *Geoph. Astroph. Fluid Dyn.*, 106 (2), 113, 2011.

19 Afanasyev, Y. D., Rhines, P. B., and Lindahl, E. G.: Velocity and potential vorticity fields
20 measured by altimetric imaging velocimetry in the rotating fluid, *Exp. Fluids*, **47**, 913, 2009.

21 Bastin, M.E., and Read, P. L.: A laboratory study of baroclinic waves and turbulence in an
22 internally heated rotating fluid annulus with sloping endwalls. *J. Fluid Mech.*, 339, 173–198,
23 1997.

24 Bastin, M. E., and Read, P. L.: Experiments on the structure of baroclinic waves and zonal
25 jets in an internally heated rotating cylinder of fluid. *Phys. Fluids*, 10, 374–389, 1998.

1 Berloff, P., Kamenkovich, I., and Pedlosky, J.: A model of multiple zonal jets in the oceans:
2 dynamical and kinematical analysis, *J. Phys. Oceanogr.*, 39, 2711–2734, 2009a.

3 Berloff, P., Kamenkovich, I., and Pedlosky, J.: A mechanism of formation of multiple zonal
4 jets in the oceans, *J. Fluid Mech.*, 628, 395–425, 2009b.

5 Centurioni, L. R., Ohlmann, J. C., and Niiler, P. P.: Permanent meanders in the California
6 Current System, *Phys. Oceanography*, 38, 1690, 2008.

7 Collin de Verdieres, A.: Mean flow generation by topographic Rossby waves, *J. Fluid Mech.*,
8 94, 39-64, 1979.

9 Fernando, H. J. S., Chen, R. R., and Boyer, D. L.: Effects of rotation on convective
10 turbulence. *J. Fluid Mech.*, 228, 513, 1991.

11 Griffiths, R. W., and Linden, P. F.: The stability of buoyancy-driven coastal currents. *Dyn.*
12 *Atmos. Oceans*, 5, 281-306, 1981.

13 Hide, R., and Mason, P. J.: Sloping convection in a rotating fluid. *Adv. in Phys.*, 24, 47–99,
14 1975.

15 Ivanov, L. M., Collins, C. A., and Margolina, T. M.: System of quasi-zonal jets off California
16 revealed from satellite altimetry, *Geoph. Res. Lett.*, 36, L03609, doi:10.1029/2008GL036327,
17 2009.

18 Kraichnan, R.: Inertial ranges in two-dimensional turbulence, *Phys. Fluids*, 10, 1417, 1967.

19 Marcus, P. S., and Lee, C.: A model for eastward jets in laboratory experiments and planetary
20 atmospheres, *Phys. Fluids*, 10, 1474, 1998.

21 Mason, P. J.: Baroclinic waves in a container with sloping endwalls. *Phil. Trans R. Soc.*
22 *Lond.*, A278, 397–445, 1975.

23 Matulka, A. M., and Afanasyev, Y. D.: Zonal jets in equilibrating baroclinic instability on the
24 polar beta-plane: experiments with altimetry, *JGR-Oceans*, 2015.

25 Maximenko, N. A., Bang, B., and Sasaki, H.: Observational evidence of alternating zonal jets
26 in the world ocean, *Geoph. Res. Lett.*, 32, L12607, doi:10.1029/2005GL022728, 2005.

27 Maximenko, N. A., Melnichenko, O. V., Niiler, P. P., and Sasaki, H.: Stationary mesoscale
28 jet-like features in the ocean, *Geoph. Res. Lett.*, 35, L08603, doi:10.1029/2008GL033267,
29 2008.

1 Maxworthy, T., and Narimousa, S.: Unsteady, turbulent convection into a homogeneous,
2 rotating fluid, with oceanographic applications. *J. Phys. Oceanogr.*, 24, 865-887, 1994.

3 Phillips, N. A.: A simple three-dimensional model for the study of large scale extra tropical
4 flow pattern. *J. Meteor.*, 8, 381–394, 1951.

5 Pratt, W. “Digital Image Processing”, Wiley-Interscience, 2007.

6 Read, P. L., Yamazaki, Y. H., Lewis, S. R., Williams, P. D., Wordsworth, R., Miki-
7 Yamazaki, K., Sommeria, J., Didelle, H., and Finchman, A.: Dynamics of convectively driven
8 banded jets in the laboratory, *J. Atmos Sci.*, 64, 4031, 2007.

9 Read, P. L., Jacoby, T. N. L., Rogberg, P. H. T., Wordsworth, R. D., Yamazaki, Y. H., Miki-
10 Yamazaki, K., Young, R. M. B., Sommeria, J., Didelle, H., and Viboud, S.: An experimental
11 study of multiple zonal jet formation in rotating, thermally driven convective flows on a
12 topographic beta-plane. *Phys. of Fluids*, 27, 085111, doi: 10.1063/1.4928697, 2015.

13 Rhines, P. B.: Waves and turbulence on a beta-plane, *J. Fluid Mech.*, 69(3), 417, 1975.

14 Rhines, P.B., Lindahl, E.G., Mendez, A.J.: Optical Altimetry: A new method for observing
15 rotating fluids with application to Rossby waves on a polar beta-plane. *J. Fluid Mech.*, 572:
16 389–412, 2006.

17 Scott, R.B., Wang, F.: Direct Evidence of an Oceanic Inverse Kinetic Energy Cascade from
18 Satellite Altimetry. *J. Phys. Oceanogr.*, **35**, 1650–1666, 2005.
19 doi: <http://dx.doi.org/10.1175/JPO2771.1>

20 Slavin, A. G, and Afanasyev Y. D.: Multiple zonal jets on the polar beta plane, *Phys. A.*
21 *Fluids*, 24, 016603, doi:10.1063/1.3678017, 2012.

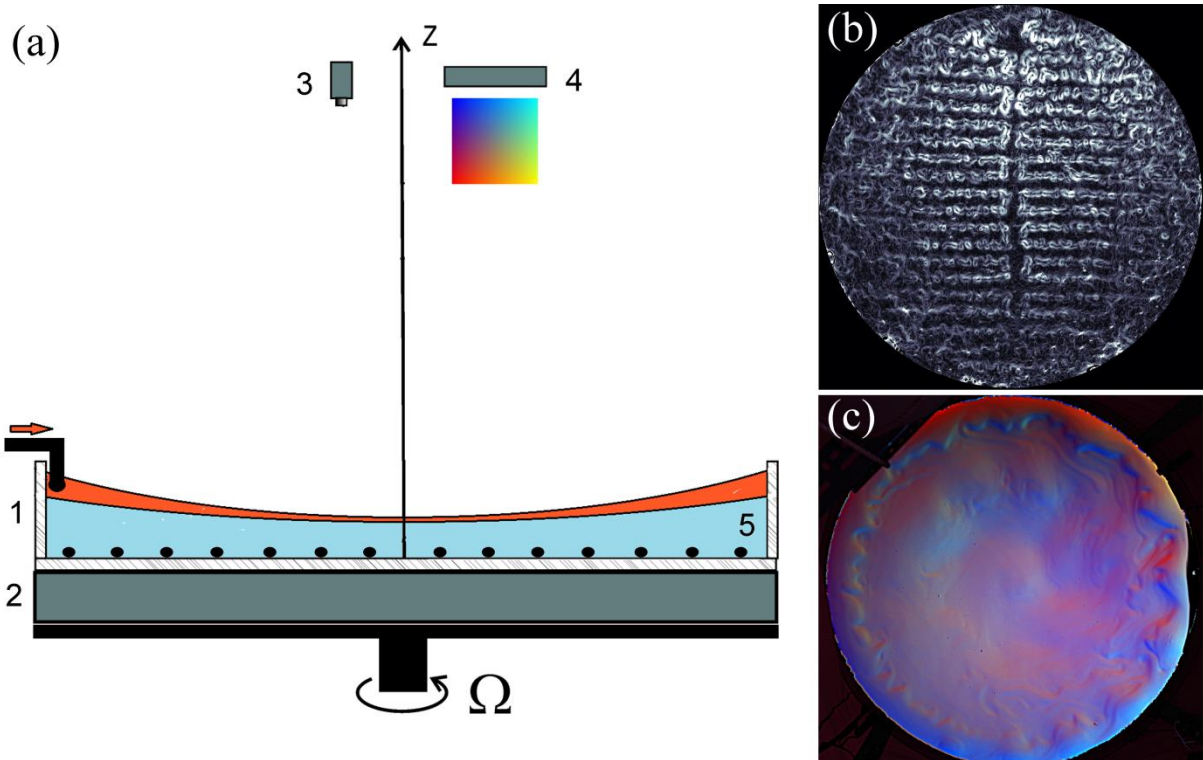
22 Smith, C. A., Speer, K. G., and Griffiths, R. W.: Multiple zonal jets in a differentially heated
23 rotating annulus, *J. Phys. Oceanogr.*, 44, 2273–2291, 2014.

24 Sommeria, J., Meyers, S. D., and Swinney, H. L.: Laboratory simulation of Jupiter’s great red
25 spot, *Nature*, 331, 689, 1988.

26 Sommeria, J., Meyers, S. D., and Swinney, H. L.: Laboratory model of a planetary eastward
27 jet, *Nature*, 337, 58, 1989.

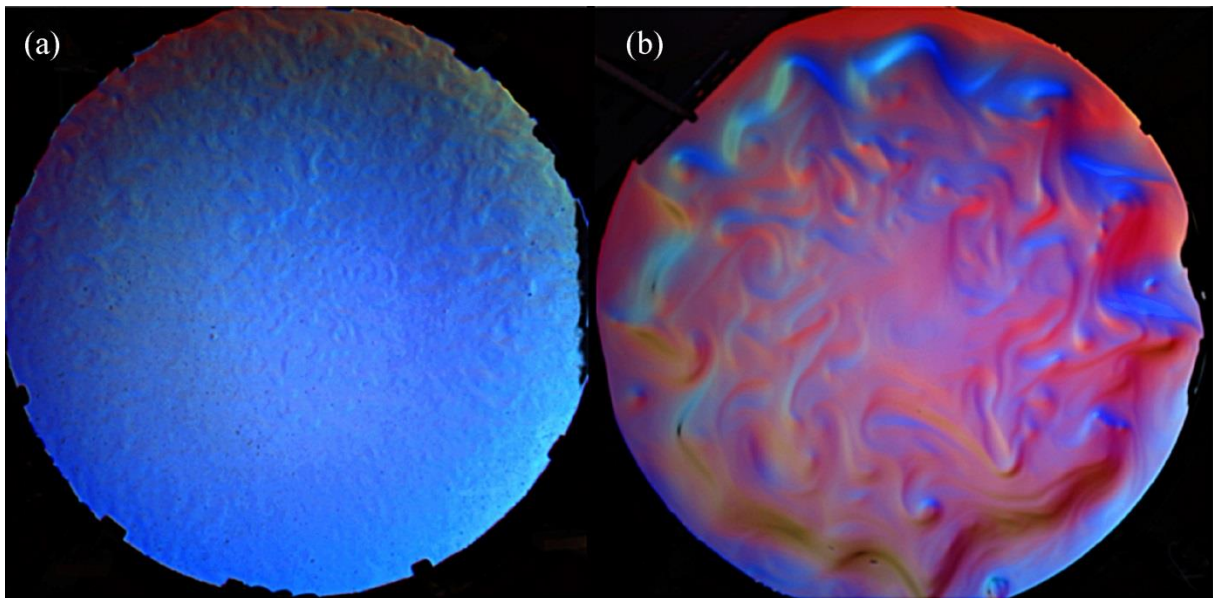
28 Vallis, G. K., amd Maltrud, M. E.: Generation of mean flows and jets on beta plane and over
29 topography, *J. Phys. Ocean*, 23, 1351, 1993.

- 1 Whitehead, J. A.: Mean flow driven by circulation on a β -plane, *Tellus*, 27, 358, 1975.
- 2 Wordsworth, R. D., Read, P. L., and Yamazaki, Y. H. 2008. Turbulence, waves and jets in a
3 differentially heated rotating annulus experiment. *Phys. Fluids*, 20, 126602, doi:
4 10.1063/1.2990042.
- 5 Yamazaki, K., Young, R. M. B., Sommeria, J., Didelle, H., and Viboud, S.: An experimental
6 study of multiple zonal jet formation in rotating, thermally driven convective flows on a
7 topographic beta-plane, *Phys. Fluids*, 27, 085111, doi:10.1063/1.4928697, 2015.
- 8 Yuan, L., and Hamilton, K.: Equilibrium dynamics in a forced-dissipative f-plane shallow
9 water system, *J. Fluid Mech.*, 280, 369, 1994.
- 10 Zhang, Y., and Afanasyev, Y. D.: Beta-plane turbulence: Experiments with altimetry, *Phys. of*
11 *Fluids*, 26, 026602, doi:10.1063/1.4864339, 2014.



1
2
3
4
5
6
7
8

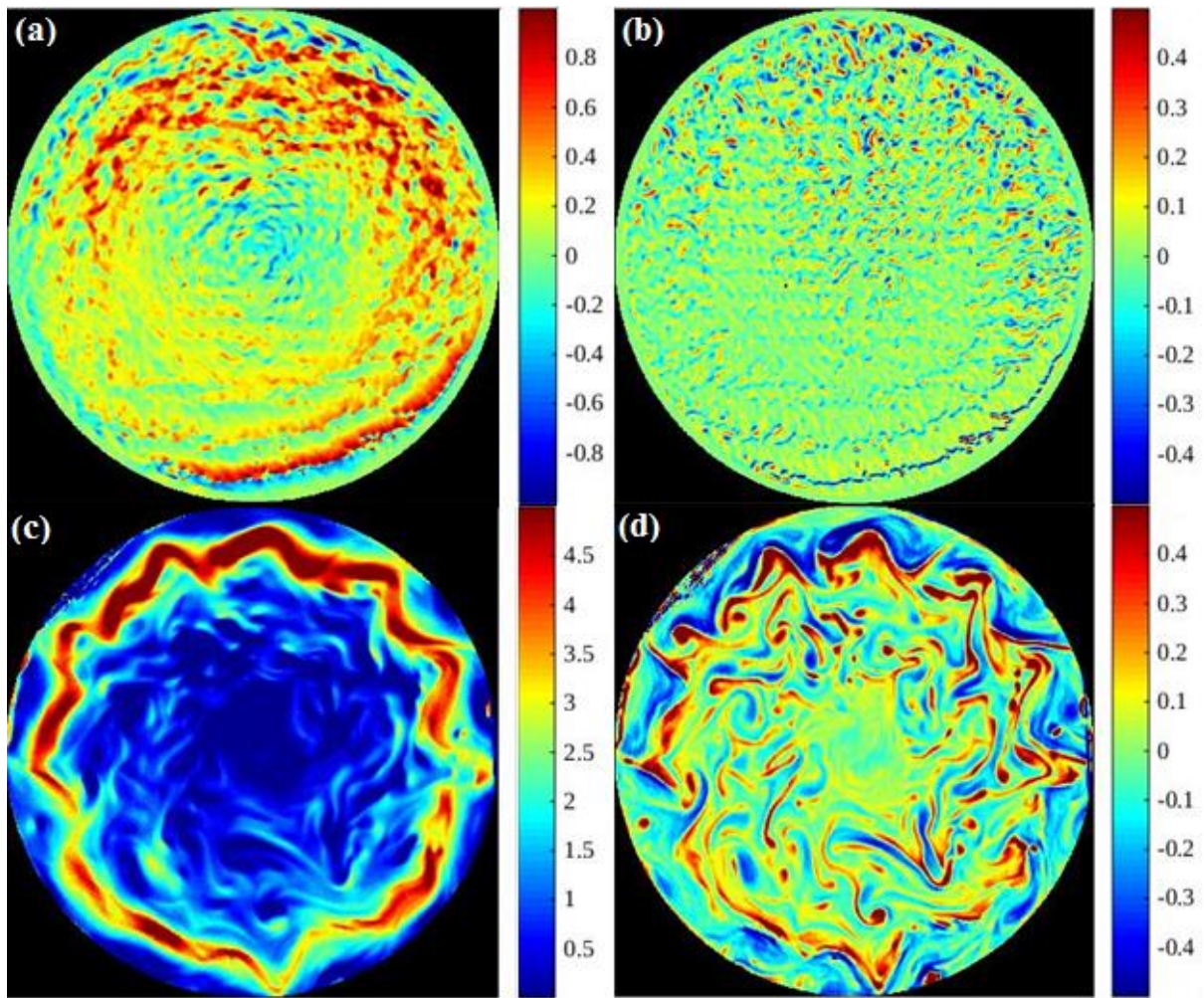
Figure 1. Sketch of the experimental setup (a) and view of the flow in the beginning of the experiments with the thermal (b) and saline (c) forcing: (1) cylindrical tank filled with water and installed on a table rotating with angular velocity Ω ; (2) light box for the optical thickness measurements; (3) video camera; (4) light source with color mask; and (5) heating wire on the bottom.



1

2

3 Figure 2. Typical images from video sequences recorded in the experiments with thermal (a)
4 and saline (b) forcing. The flows are visualized by optical altimetry (AIV); different colors
5 indicate different values (both in magnitude and direction) of the gradient of the surface
6 elevation.

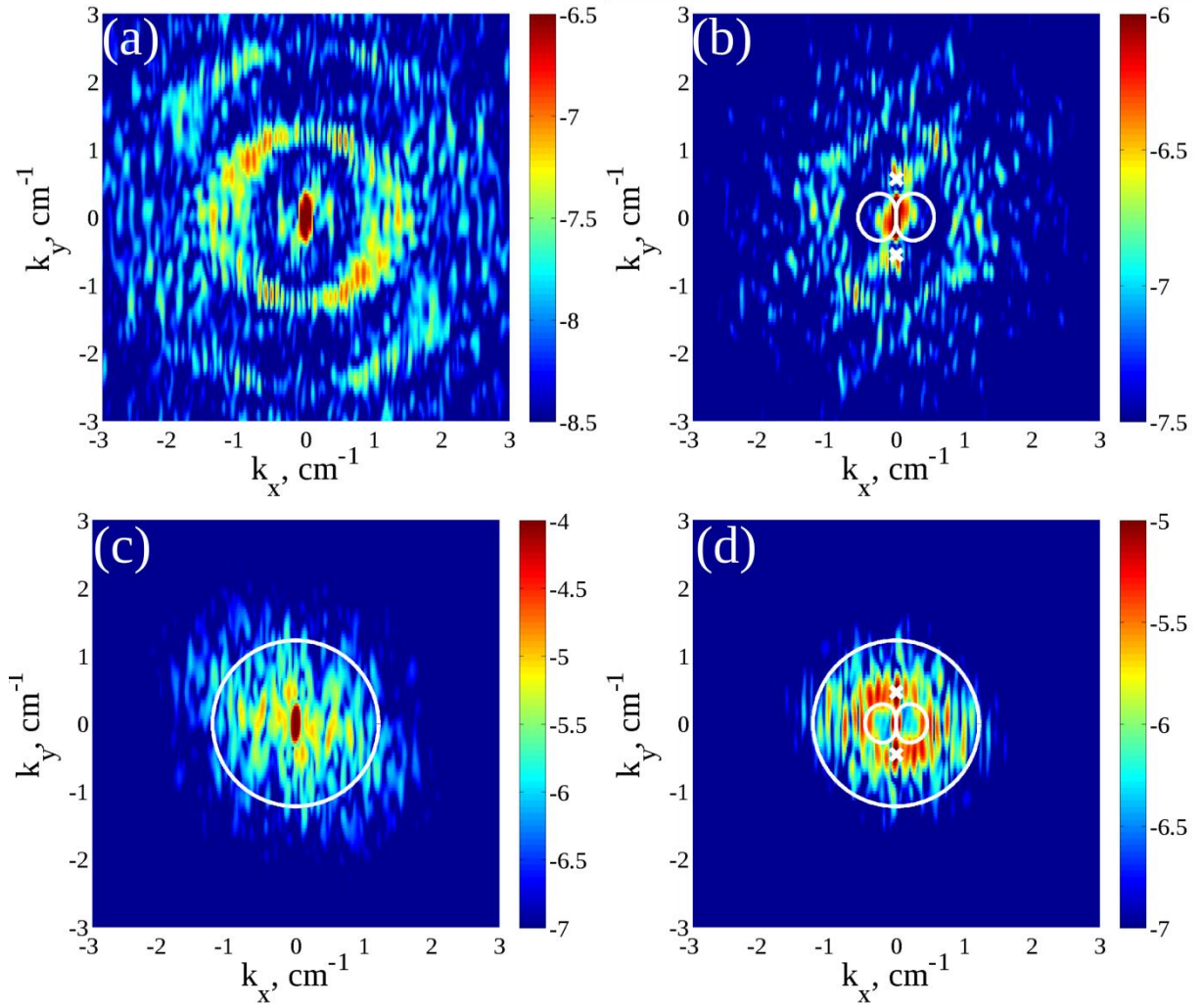


1

2

3 Figure 3. Flows generated by thermal forcing at $t = 280$ s (a, b) and by saline forcing at $t = 150$
 4 s (c, d). Panels (a) and (c) show the x-component of velocity (azimuthal velocity) u while
 5 panels (b) and (d) show the dimensionless relative vorticity, ζ / f_o . Salinity difference
 6 between the layers for the experiment with saline forcing (a, b) is $S = 30$ ppt. The center of the
 7 tank corresponds to the North Pole of the polar β -plane.

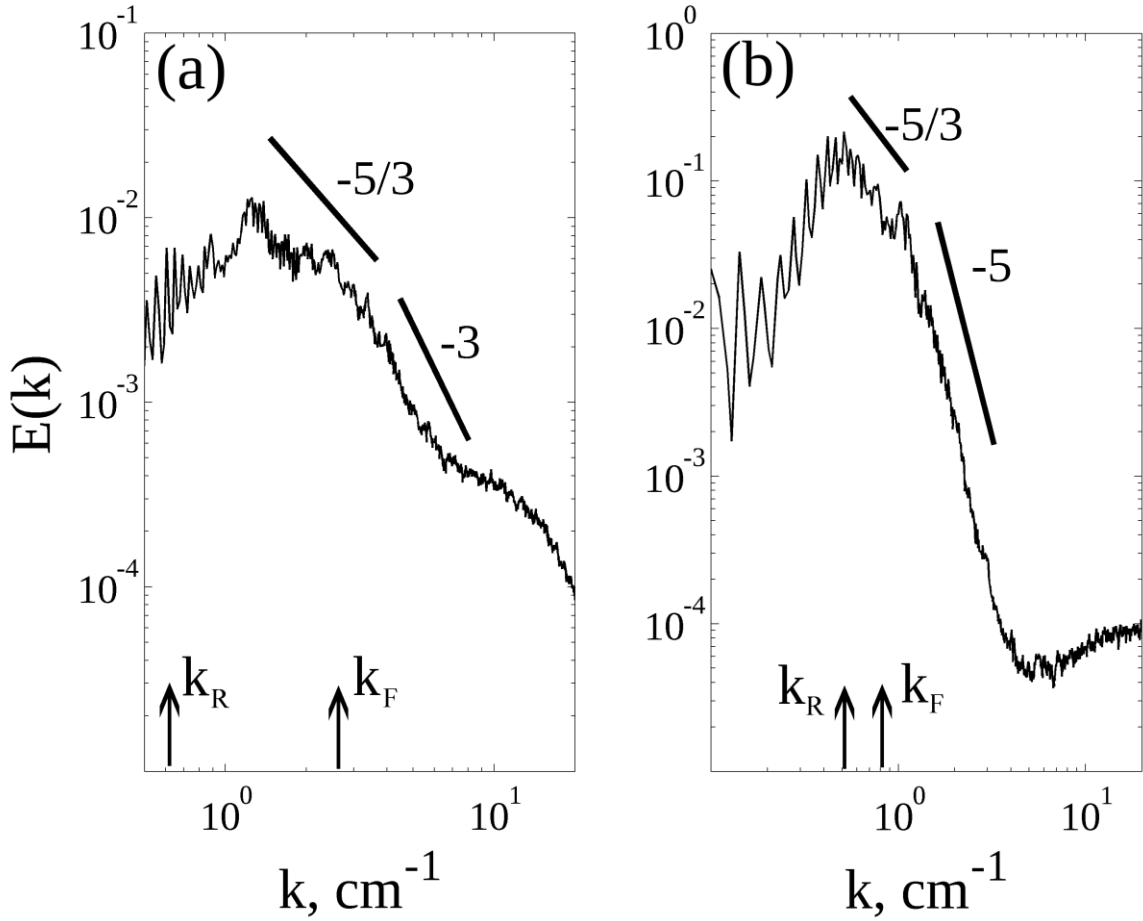
8



1

2

3 Figure 4. Energy spectra in the wavenumber space (k_x, k_y) for the experiments with thermal (a,
 4 b) and saline (c, d) forcing: $t = 30$ s (a) 630 s (b) from the beginning of the thermal
 5 experiment; $t = 10$ s (c) 722 s (d) after the fresh water source stopped in the experiment with
 6 saline forcing. Color shows energy in logarithmic scale. Black circles in (c) and (d) show R_d^{-1} .
 7 Black crosses in (b) and (d) represent the Rhines scale wavenumber (5) while the dumbbell-
 8 shaped curve is given by Eq. (6).



1
2
3
4
5

Figure 5. The one-dimensional energy spectra in log-log scale for the experiments with thermal (a) and saline (b) forcing: $t = 630$ s (a) 722 s (b) (as in Fig. 4 (b, d)).